Tecnociencia 2006, Vol. 8, N° 1.

A METHODOLOGY FOR FILTERING AND INVERSION OF SURFACE WAVES: AN EXAMPLE OF APPLICATION TO THE LITHOSPHERIC STRUCTURE DETERMINATION OF THE SOUTH IBERIA

Victor Corchete
Higher Polytechnic School, University of Almeria, 04120 ALMERIA, Spain.
e-mail: corchete@ual.es , Fax +34 950 015477.

ABSTRACT

Most important features of the earth structure can be studied through the analysis of Rayleigh wave dispersion. This consists on its filtering and inversion to obtain shear wave velocity distribution with depth. I have applied this analysis to show lithospheric structure of South Iberia, by means of a set of 2D images of shear velocity for depths ranging from 1.5 to 46 km. The data used to obtain Rayleigh wave dispersion are the traces of 44 earthquakes, occurred on the neighbouring of Iberia. These earthquakes have been registered at 3 WWSSN stations located on Iberia. These stations have been considered because period range of best registration for WWSSN seismograph is the more suitable to explore the elastic structure of the Earth, for the depth range which is the objective of this study. I have proceeded to group all seismic events in source zones to obtain a dispersion curve for each path source-station. Dispersion curves are obtained by digital filtering with a combination of MFT and TVF filtering techniques. Thus, a set of source-station averaged dispersion curves was obtained. This set of dispersion curves is inverted according to generalized inversion theory, to obtain shear wave velocity models for each source-station path. These models can be interpolated to obtain a 2D mapping of the elastic structure of South Iberia, by kriging method. This mapping reveals the principal structural features of South Iberia and surroundings zones. Such features, as the existence of lateral and vertical heterogeneity in the study area, also can be seen in Moho depth mapping presented in this paper. Finally, I want to remark that no shear velocity models have been obtained for intermediate depths (5 to 30 km), up to date, for the Iberian area. For this reason, this is the goal of the study presented in this paper.

KEYWORDS
MFT, TVF, Inversion, Rayleigh waves, Lithosphere, South Iberia.

RESUMEN
Las características más importantes de la estructura terrestre pueden ser estudiadas por medio del análisis de la dispersión de las ondas Rayleigh. Este análisis consiste en filtrado e inversión para obtener la distribución de velocidad de la onda de cizalla con la profundidad. Como ejemplo, se ha aplicado este análisis para mostrar la estructura litosférica del sur de Iberia, por medio de un conjunto de imágenes 2D de la velocidad de cizalla para profundidades que van desde 1.5 a 46 km. Los datos usados para obtener la dispersión de ondas Rayleigh han sido las trazas de 44 terremotos, ocurridos en las proximidades de Iberia. Estos terremotos han sido registrados en 3 estaciones WWSSN situadas en Iberia. Estas estaciones han sido elegidas porque el rango de periodo en el cual registra mejor el sismógrafo WSSSN, es el más adecuado para explorar la estructura terrestre, dentro del rango de profundidad que es objetivo de este estudio. He procedido a agrupar todos los eventos sísmicos en zonas fuente para obtener una curva de dispersión para cada trayectoria fuente-estación. Las curvas de dispersión son obtenidas por filtrado digital con una combinación de las técnicas de filtrado MFT y TVF. Así, obtengo un conjunto de curvas de dispersión fuente-estación. Este conjunto de curvas de dispersión es invertido de acuerdo con la teoría de la inversión generalizada, para obtener modelos de velocidad de onda de cizalla para cada trayecto fuente-estación. Estos modelos pueden ser interpolados para obtener un mapa 2D de la estructura elástica del sur de Iberia, por el método de kriging. Este mapa revela las principales características estructurales del sur de Iberia y zonas próximas. Tales características, como la existencia de lateral y vertical heterogeneidad en el área de estudio, también pueden ser vistas en el mapa de profundidad del Moho presentado en este artículo. Finalmente, quiero señalar que, hasta la fecha, no se han obtenido nunca modelos de velocidad de cizalla para el rango de profundidad intermedia considerado en este estudio (desde 5 a 30 km), en el área ibérica. Por ello, este es el objetivo del estudio presentado en este artículo.

PALABRAS CLAVES
MFT, TVF, Inversión, ondas Rayleigh, Litosfera, Sur de Iberia.

INTRODUCTION

As it is well know, surface waves show dispersion along the propagation path and this dispersion is related to the Earth structure crossed by the waves. This basic property allows using of dispersion analysis techniques as a tool to study important features of the Earth structure. Such kind of analysis consists on filtering and inversion of surface waves to obtain shear wave velocity versus depth. A pioneer

study of dispersion analysis carried out in the Iberian Peninsula, by Payo (1965), was an estimation of Rayleigh wave dispersion along a path between the two WWSSN stations at Toledo and Malaga, to obtain the first shear velocity model for Iberia. Later, several shear velocity models have been obtained for this study area for deep structure with depths raging 30 to 250 km (Badal et al., 1990; Corchete et al., 1993, 1995) and for shallow depths from 0 to 5 km (Navarro et al., 1997; Chourak et al., 2001, 2003). Nevertheless, no shear velocity models have been obtained for intermediate depths (5 to 30 km); this is the goal of the study presented in this paper. Thus, the purpose of this paper is to show the South Iberian lithosphere structure by means of a set of 2D images of shear velocity for depths ranging from 1.5 to 46 km. This study will be completed in the future by the obtaining of a set of images for the Northern part of Iberia.

Data set

44 earthquakes occurred in the neighbouring of Iberia, have been considered in this study (Table 1). These earthquakes have been registered at 3 WWSSN stations located in this region. I considered LP instruments of the WWSSN stations because the period range of best registration for these seismographs is between 5 to 45 s, as it can be seen in the Figure 1.

Table 1. List of events used in this study.

Event nº	Date D M Y	Origin Time Hr Min Sec	Location Lat (ºN)	Long (ºE)
1	04 09 1963	05 06 42.0	36.000	5.200
2	15 11 1964	20 03 52.0	34.800	- 5.400
3	07 09 1965	06 16 47.0	35.200	4.500
4	26 08 1966	05 56 19.0	38.100	- 8.600
5	27 05 1967	01 54 24.0	35.700	- 0.200
6	13 07 1967	02 10 24.0	35.400	- 0.200
7	06 03 1969	19 23 43.0	36.200	- 10.700
8	20 04 1969	16 12 13.0	35.800	- 9.200
9	05 05 1969	05 34 25.0	36.000	- 10.300
10	06 09 1969	14 30 35.0	36.900	- 12.000
11	30 12 1970	20 57 29.0	37.100	- 14.500
12	16 03 1972	21 31 33.0	37.400	- 2.300
13	18 04 1972	05 51 51.0	36.300	- 11.200
14	24 08 1973	10 50 57.0	36.000	- 2.100
15	24 11 1973	15 22 09.0	36.100	4.400
16	24 11 1973	14 05 49.0	36.100	4.400
17	25 11 1973	04 20 25.0	36.100	4.400
18	28 06 1974	11 09 35.0	36.300	5.300
19	29 06 1974	01 06 52.3	36.300	5.200
20	13 07 1974	15 57 20.0	35.900	4.700
21	14 04 1977	07 17 10.1	36.180	5.360
22	14 08 1978	14 17 50.3	36.300	- 7.000
23	09 05 1980	09 21 36.7	35.430	1.100
24	13 10 1980	14 33 48.2	36.280	1.290
25	14 10 1980	17 35 02.1	36.220	1.330
26	15 10 1980	03 17 24.7	36.190	1.290
27	19 10 1980	21 47 24.2	35.510	1.200
28	22 10 1980	16 23 15.8	36.220	1.280
29	23 10 1980	09 57 56.7	36.350	1.320
30	30 10 1980	23 38 14.9	36.180	1.340
31	01 02 1981	23 00 42.0	36.370	1.640
32	05 02 1981	09 12 33.2	36.350	1.440
33	14 02 1981	13 15 18.0	35.850	1.220
34	20 02 1981	20 41 02.9	35.400	1.180
35	19 04 1981	19 29 35.4	35.510	-0.240
36	11 09 1982	21 35 51.9	36.320	1.600
37	11 09 1982	04 48 41.6	35.560	1.310
38	15 11 1982	20 07 52.4	35.590	1.250
39	24 01 1983	16 34 09.4	39.720	- 14.480
40	31 03 1984	03 31 56.0	36.410	1.520
41	27 10 1985	19 34 59.7	36.380	6.710
42	12 02 1989	12 02 21.6	36.330	2.600
43	12 04 1990	22 47 55.6	36.740	2.480
44	19 01 1992	20 21 33.1	36.090	1.520

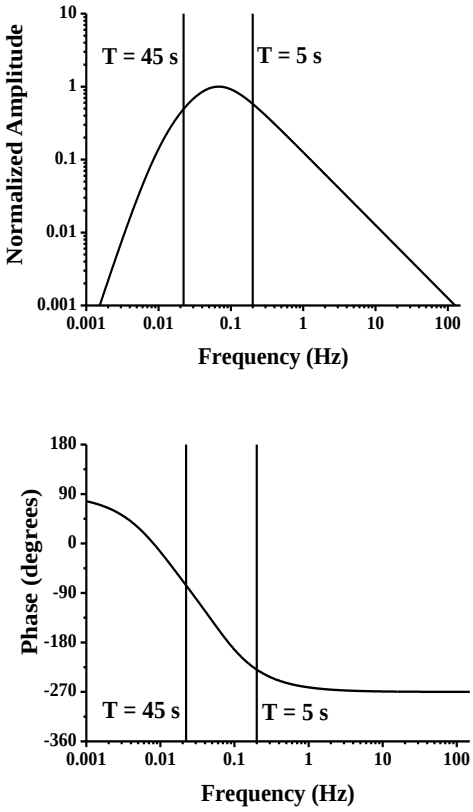

Fig. 1. Frequency dependent response characteristics for LP-WWSSN seismograph system.

This range of period is the more suitable to explore the elastic structure of the Earth, for a depth range which is the objective of this study (from 5 to 30 km of depth, approximately).

Only were considered traces in which a well-developed Rayleigh wave train is present, with a very clear dispersion, to ensure the reliability of the results of this study (Fig. 2). Logically, instrumental response must be taken to account to avoid the time lag introduced by the seismograph system. This time lag can be appreciated in Figure 2. In this Figure we also can see the magnification of short period produced after application of the instrument correction. This magnification

recovers the true amplitude of this range of period and allow us to analyse the short period dispersion with more reliability. For both reasons, all the traces considered in this study were corrected for instrument response.

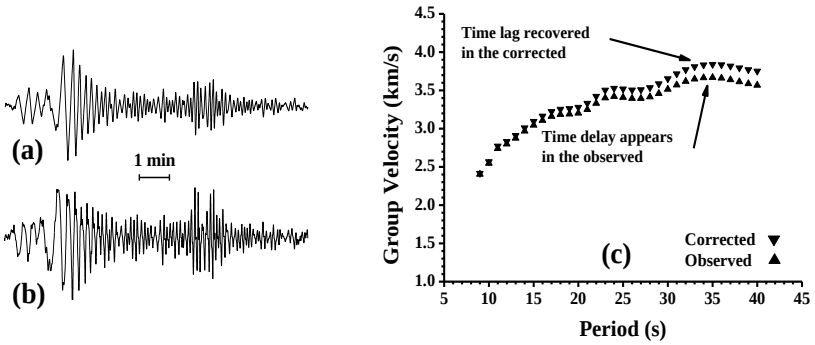

Fig. 2. (a) Observed seismogram corresponding to the vertical component of the Rayleigh wave due to the event 16 (as listed in Table 1). This trace was recorded at EBR station (as listed in Table 2). (b) The above seismogram with instrumental correction. (c) Dispersion curves of both seismograms (plotted in (a) and (b)) show the time lag produced by the seismograph system.

Grouping seismic events in source zones

Rayleigh waves propagating along very near epicentre-station paths show quite similar dispersion curves, because the waves cross the same Earth structure and the elastic properties of the medium are also the same. Thus, all seismic events listed in Table 1 were grouped in source zones as listed in Table 3. These source zones are defined as a location in which have occurred seismic events with similar epicentre coordinates. The coordinate differences for a group of events in the same source zone, must be less than or equal to 0.2 degrees in latitude and longitude. By this procedure, a dispersion curve for each path source-station was obtained and it is listed in Table 4, when are averaged the dispersion curves obtained analysing each trace of the event registered at this station. I obtain also small deviations considered as errors that can be described by the standard deviation. Figure 3 shows the path coverage of the study area, as a result of the above described criteria for grouping of the events.

Table 2. List of WWSSN stations used in this study.

Station code	Latitude (ºN)	Longitude (ºE)
EBR	40.821	0.493
MAL	36.728	-4.411
TOL	39.881	-4.049

Table 3. List of source zones used in this study.

Zone code	Latitude (ºN)	Longitude (ºE)
S1	36.000	5.200
S2	35.200	4.500
S3	38.100	-8.600
S4	35.700	-0.200
S5	35.400	-0.200
S6	36.200	-10.700
S7	35.800	-9.200
S8	36.000	-10.300
S9	36.900	-12.000
S10	37.100	-14.500
S11	37.400	-2.300
S12	36.300	-11.200
S13	36.000	-2.100
S14	36.100	4.400
S15	36.300	5.300
S16	35.900	4.700
S17	36.300	-7.000
S18	35.430	1.096
S19	36.276	1.288
S20	36.370	1.640
S21	35.850	1.220
S22	35.560	1.310
S23	36.380	6.710
S24	36.330	2.600
S25	36.740	2.480
S26	36.090	1.520
S27	35.510	1.204
S28	39.720	-14.480
S29	34.800	-5.400
S30	36.220	1.330
S31	35.590	1.250

Table 4. List of paths epicentre-station crossing the study area and events involved (as listed in Table 1, 2 and 3).

Path	Events
S1-TOL	1
S2-TOL	3
S3-TOL	4
S4-TOL	5,35
S5-TOL	6,35
S6-TOL	7
S7-TOL	8
S8-TOL	9
S9-TOL	10
S10-TOL	11
S11-TOL	12
S12-TOL	13
S13-TOL	14
S14-TOL	15,16,17
S15-TOL	18,19
S16-TOL	20
S17-TOL	22
S18-TOL	23,27,34,38
S19-TOL	24,25,26,28,29,30,32
S20-TOL	31,32,36,40
S21-TOL	33
S22-TOL	37,38
S23-TOL	41
S24-TOL	42
S25-TOL	43
S26-TOL	25,30
S10-EBR	11
S11-EBR	12
S14-EBR	15,16,17
S15-EBR	18,19,21
S16-EBR	20
S19-EBR	24,25,26,28,29,30
S27-EBR	27,37
S21-EBR	33
S28-EBR	39
S25-EBR	43
S26-EBR	25,30,44
S1-MAL	1
S29-MAL	2
S3-MAL	4
S4-MAL	5
S5-MAL	6
S12-MAL	13
S15-MAL	18,19
S30-MAL	25,28,29,30
S31-MAL	38
S28-MAL	39
S23-MAL	41

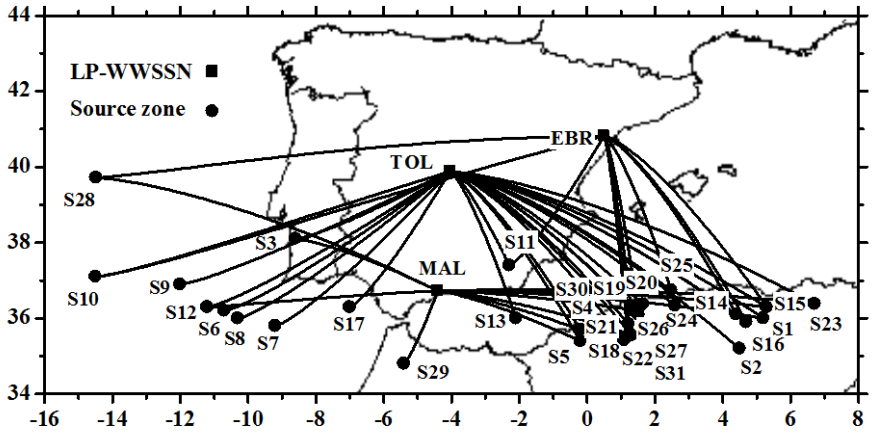

Fig. 3. Iberian area covered by the Rayleigh waves.

Dispersion analysis

Once the events were grouped was obtained the Rayleigh wave group velocity dispersion curves for the trace of each event registered, by means of applying digital filtering techniques. MFT (Multiple Filter Technique) and TVF (Time Variable Filtering) were used to obtain the group velocity dispersion curve, as it is show in the flow chart displayed in Figure 4.

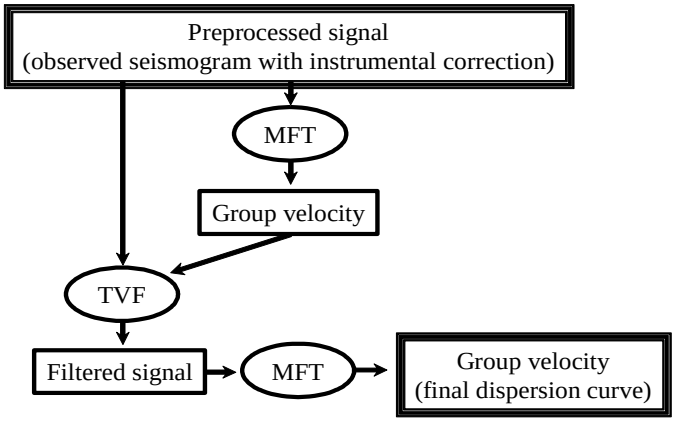

Fig. 4. Steps followed in the filtering process of each event-station seismogram to obtain its dispersion curve. Circles are used to denote the application of a digital filtering technique and rectangles are used to denote the results obtained. Enhanced rectangles are used to show initial data and final results.

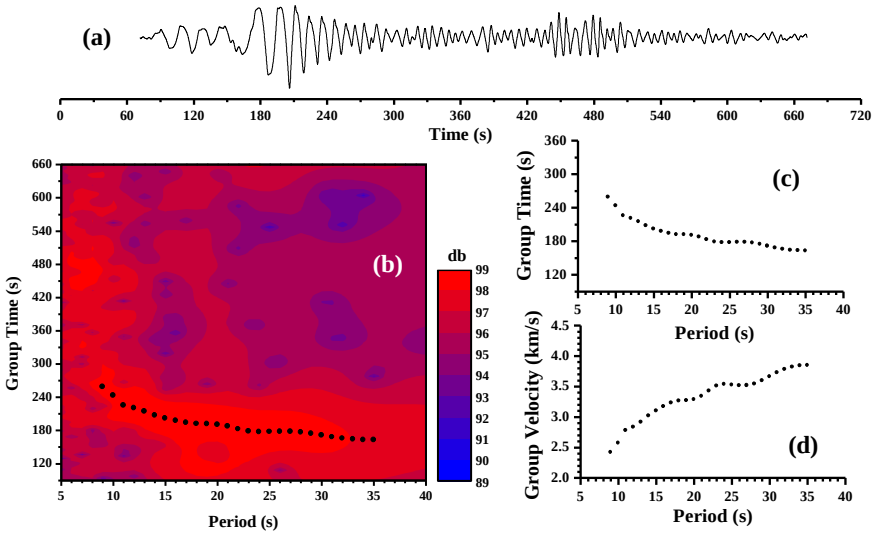

Fig. 5. (a) Observed seismogram corresponding to the event 16 (as listed in Table1) recorded at EBR station, instrument corrected. (b) Contour map of relative energy normalized to 99 decibels, as a function of period and group time (points denote group times inferred from the energy map). (c) Group time curve inferred from the energy map. (d) Group velocities calculated from the group times and epicentral distance (group velocity is the epicentral distance divided by the group time for each period).

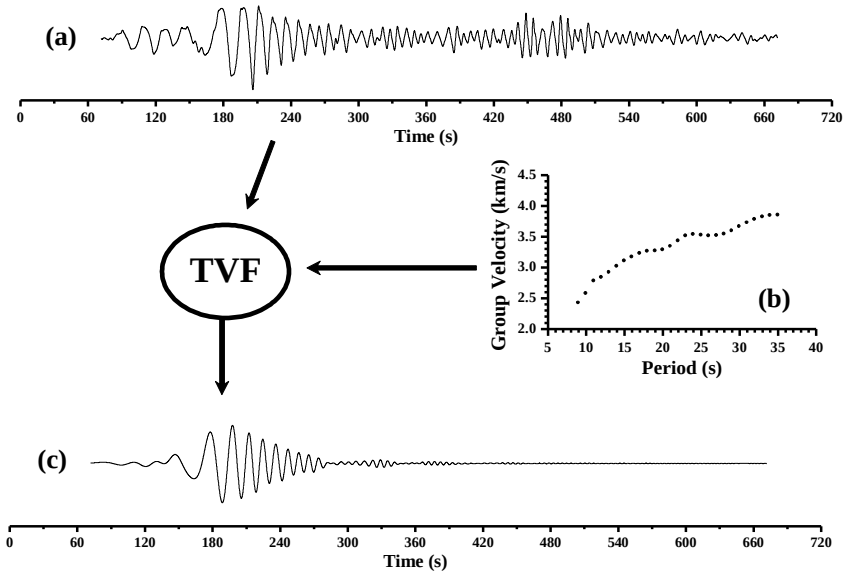

Fig. 6. (a) Observed seismogram corresponding to the event 16 (as listed in Table1) recorded at EBR station, instrument corrected. (b) Group velocity dispersion curve obtained after application of MFT as it is show in Figure 5. (c) Time-variable filtered seismogram.

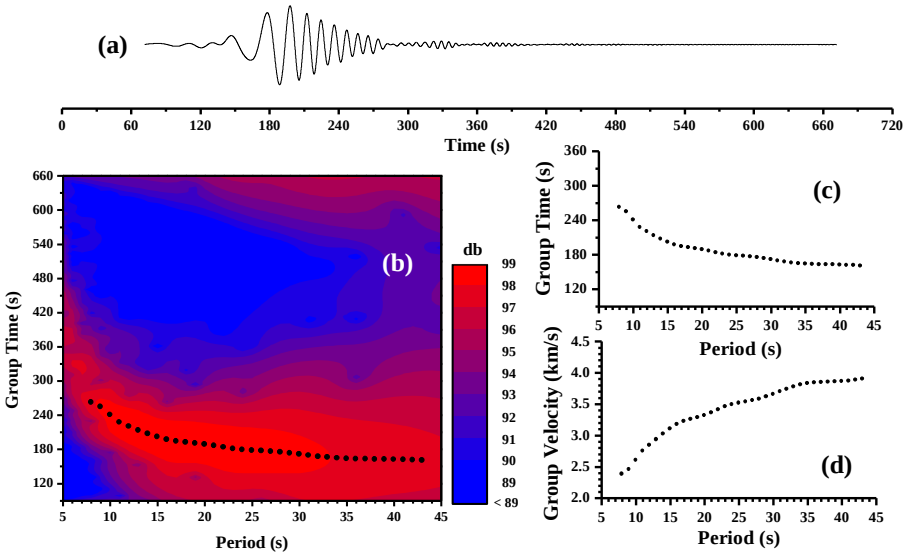

Fig. 7. (a) Time-variable filtered seismogram obtained after application of TVF as it is show in Figure 6. (b) Contour map of relative energy normalized to 99 decibels, as a function of period and group time (points denote group times inferred from the energy map). (c) Group time curve inferred from the energy map. (d) Group velocities calculated from the group times and epicentral distance.

As an example, the filtering process described above was applied to the event 16 (as listed in Table 1) corresponding to S14-EBR path. This trace was previously corrected of the instrumental effect as it is shown in Figure 2; next, I applied MFT (Dziewonski *et al*., 1969; Corchete *et al*., 1989) to this trace as it is shown in Figure 5. The dispersion curve obtained plus this trace are used to obtain the digital filtered signal by using TVF (Cara, 1973; Corchete *et al*., 1989). Figure 6 show the time-variable filtered signal as a result of TVF. Finally, in Figure 7 we can see the final dispersion curve obtained after application of MFT to the filtered signal (as it was showed in the flow chart of Figure 4).

A comparison between Figures 5 and 7 indicates that the filtering process I propose in this paper (and displayed in Figure 4) works better than the application of MFT only. Contour maps of relative energy plotted in Figures 5b and 7b, show the improved achieved after application of TVF combined with MFT versus the application of MFT to the observed seismogram without TVF. Period range has been

increased in the group velocity dispersion curve after application of MFT to the time-variable filtered signal, versus the application of MFT to the observed signal, as it can be seen when we compare Figures 5d and 7d. Dispersion curve obtained after application of MFT only, reach to a maximum period of 35 seconds whereas the maximum period reached in the dispersion curve showed in Figure 7d is 44 seconds. Moreover, the group velocity dispersion curve plotted in Figure 5d is not as smooth as this plotted in Figure 7d which is determined by the proposal process of filtering (MFT and TVF combined). Considering the improvements mention above, this filtering process is revealed as a powerful tool for dispersion analysis. For this reason, this filtering process is considered today as a standard tool for dispersion analysis in long and short period (Badal et al., 1996; Chourak et al., 2003).

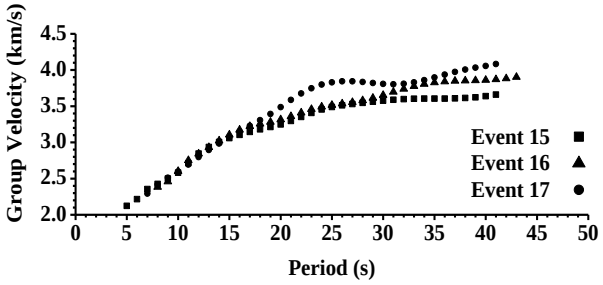

(a)

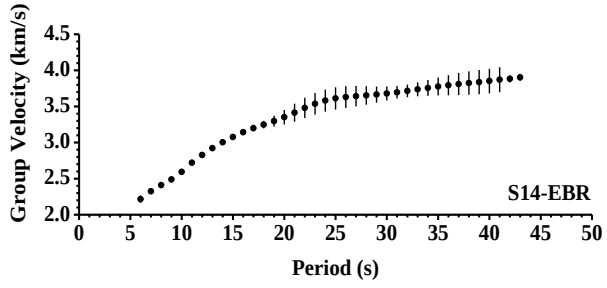

(b)

Fig. 8. (a) Group velocity dispersion curves obtained after application of MFT and TVF, following the filtering process displayed in Figure 4 to each trace of the events 15, 16 and 17 (as listed in Table 1). (b) Path-average dispersion curve for S14-EBR path (as listed in Table 4) calculated from the group velocities plotted in Figure 8a. Dots denote average group velocity and vertical bars show the standard deviation at each period (1-σ errors).

Once all dispersion curves of the traces for the events involved in a path were calculated, by means of the filtering process described above, was proceed to obtain the group velocity for this path. In Figure 8, we can see as an example the path average dispersion curve for S14-EBR path. For each event involved in this path, was calculated previously its dispersion curve, with the above-described combination of filtering techniques (MFT and TVF), obtaining after the average group velocity as a mean of the group velocity values obtained for each period. An estimation of the error for the average group velocity is obtained computing the standard deviation of the values involved in the calculation of this media. In Table 4, some paths have only one event involved. Logically, not all events are well registered in all stations; events with a bad trace were discarded in this study to ensure the reliability of the results. In this case, error estimation is a mean of the standard deviations obtained for the other paths, in which there are more than one event involved. This error is already 0.05 km/s for the paths considered in this study.

Following this procedure, was determined a dispersion curve of group velocity for each path listed in Table 4, obtaining a set of source-station averaged dispersion curves with 1-σ errors (one standard deviation). A set of dispersion curves like this, can be inverted to obtain shear wave velocity models as will be describe below, which is the goal of the present study joint to a 2D mapping of the elastic structure of the South Iberia.

Inversion process

Was followed the inversion method for surface wave dispersion detailed by Badal et al. (1992). This method was also briefly described by Badal et al. (1990), including a flow chart of this inversion process. Nevertheless, significance and principal application of the concepts as resolving kernels, forward modelling and inverse approach; are described with more detail by Badal et al. (1992). Here, was briefly described these concepts to explain how is achieved a shear velocity model for a path-average dispersion curve previously obtained, with all reliability and accuracy that it is possible to do it.

Selection of an initial model is a previous step before the inversion process. In this case, was chosen as initial earth model a mean earth model obtained by Corchete et al. (1995) for Iberia. In this model, the

Moho discontinuity was changed from 31 km to 17.5 km of depth, because theoretical dispersion curve obtained in this way is more similar to the path-average dispersion curves, than theoretical curve obtained from this model with a Moho discontinuity at 31 km depth. This change is necessary due to the inversion scheme selected, in which, only are considered small perturbations for the wave velocities involved (Badal et al., 1992). This method conditions the choice of an initial model as similar as possible to the true earth structure, represented by the path average dispersion curves and all geophysical information available for the studied area structure. The model considered here is listed in Table 5 and its shear wave velocity distribution with depth is plotted in Figure 9a. Theoretical group velocity shown in Figure 9b, is obtained by forward modelling as it is described by Aki and Richards (1980). Once the starting model was ready, was proceed to the inversion of each path-average group velocity obtained previously, to obtain the shear velocity models for each path considered. A program based on the generalized inversion theory, which flow chart is showed by Badal et al. (1990), was used. In Figure 10 is shown an example of the results of such program. In this example, S14-EBR dispersion curve was inverted. Shear velocity model shown in Figure 10a, is the final model obtained for this path, by means of an iterative process in which model is improved at each iteration. The improvement in model iteratively obtained, is checked by comparison between group velocity considered as observed data (S14-EBR dispersion curve) and theoretical dispersion curve, calculated from the actual model by forward modelling. If these curves are closer than the previous iteration, the process converges. When theoretical curve falls within the vertical error bars of the observed, as can be seen in Figure 10c, inversion process finish, because the shear velocity model obtained describes the observed curve within its experimental error.

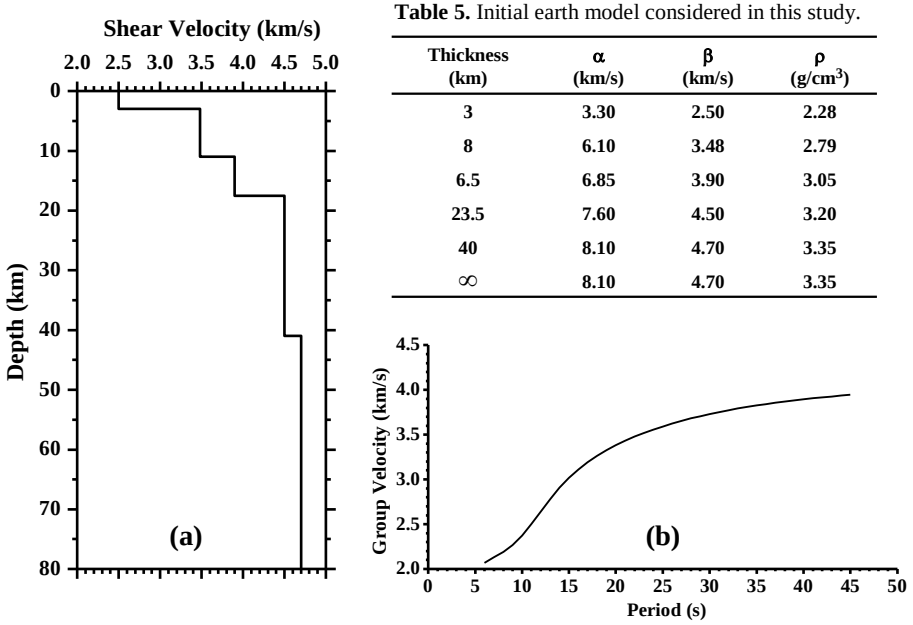

Table 5. Initial earth model considered in this study.

Thickness (km)	α (km/s)	β (km/s)	ρ (g/cm^3)
3	3.30	2.50	2.28
8	6.10	3.48	2.79
6.5	6.85	3.90	3.05
23.5	7.60	4.50	3.20
40	8.10	4.70	3.35
∞	8.10	4.70	3.35

Fig. 9. (a) Shear velocity distribution of the initial model (as listed in Table 5). (b) Theoretical group velocity obtained from the initial model listed in Table 5, by means of forward modelling.

Resolving kernels showed in Figure 10b indicate the reliability of the solution obtained to the inverse problem. Resolving kernels are row vectors of the resolution matrix and therefore a measure of the exactness in the solution of the inverse problem (Tarantola 1987). A good agreement between calculated solution and true solution (which implies the reliability of the estimated solution), is obtained when the absolute maxima of these functions fall over the reference depths. These reference depths are defined as the media depth of each layer considered in the model. This reliability is also related to the width of these absolute maxima. The solution achieved to the inversion problem is more reliable when the maxima of these resolving kernels are narrower.

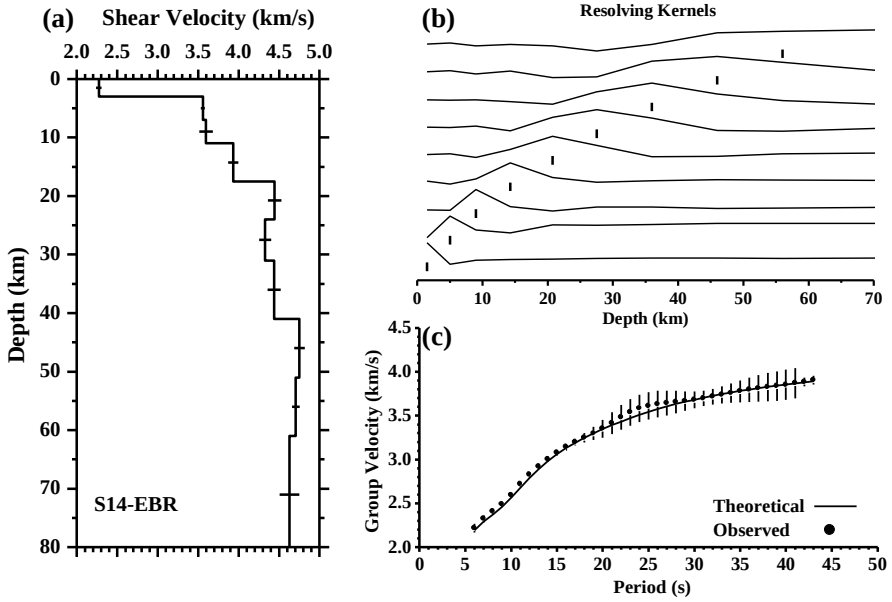

Fig. 10. (a) Shear wave velocity model obtained after inversion process for S14-EBR path. Horizontal bars show standard deviation for each layer considered in this inversion process (10 layers). (b) Resolving kernels of the inversion problem posed. Reference depths are marked by vertical bars for the depth of each layer considered. (c) Theoretical group velocity obtained from the final model plotted in Figure 10a, is showed with continuous line (labelled as theoretical). Dots line denotes average group velocity obtained for S14-EBR path (labelled as observed) and vertical bars show the standard deviation at each period (1-σ errors in the observed data).

To improve the solution reliability the number of layers considered in model to the minimum number of layers must be reduced. This is necessary to obtain a detailed shear velocity distribution with depth, as it is required to satisfy observed dispersion data within its error. If a large number of layers are considered, the number of unknowns is increased but the data are the same; as a result, resolution becomes worse. This effect is showed by resolving kernels with absolute maxima more width and a lack of coincidence between the maxima of these functions with the reference depths.

Another method to improve resolution is considering layers with thickness that increased with depth as resolution worsen. This effect can be seen in Figure 10b, resolving kernels make worse as depth increased. To avoid this effect as is possible, the layer thickness

considered in my model increases with depth. Thus, shallow layers are thinner than deeper layers, which are thicker.

Shear wave velocity mapping

Results presented in this paper involved 48 source-station paths in which has been calculated the shear velocity distribution with depth. All this widespread information is hard to handle for the geophysical interpretation without any way of mapping. For this reason, I have interpolated these data to put on a regular grid suitable for plotting with contour maps. Thus, ray paths shown in Figure 3 are converted in point data, for this, each path is divided in 9 equidistant points along this path, as it is shown in Figure 11. I have cheeked the mapping with adding more points by path, but mapping have not changed significantly. Once the ray paths have been assigned to points, I have point data of shear velocities for each layer considered in the 1-D shear velocity models. Then, I can interpolate these point data for each layer obtaining a regular data grid for each reference depth. Later I can proceed to map with contours these gridded data obtaining a 2-D image of shear velocity, for each reference depth. Such 2-D images can be more easily interpreted and correlated with geophysical and geological information, available for the study area.

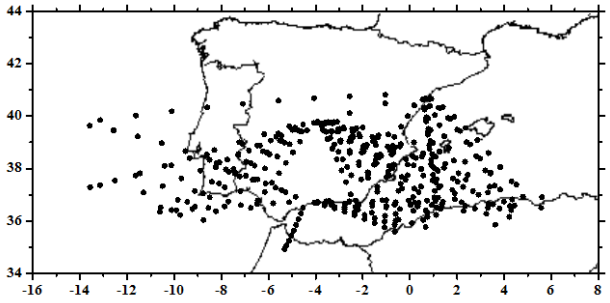

Fig. 11. Distribution of shear velocity data available for later interpolation in a regular grid.

I have used the MICROCAL software package (© 2002 MICROCAL™ Software, Inc.) for the computation of this regular data grid from the point data velocities, distributed as it is show in Figure 10b. This software package is based on a kriging routine that follows

the kriging method described by Davis (1986). A measure of guarantee and reliability of this interpolation is checked testing the gridded data values, by means of comparison between the input values and the output values predicted by this interpolation. For each reference depth, interpolation process is finished with a computation of standard deviation of the differences between the input and predicted values. After this interpolation process, is obtained the gridded data for each reference depth. The gridded data are distributed for study area in a 100x30 regular grid with a mesh size of 0.2º x 0.2º and 3000 points.

Figure 12 show the results of such interpolation process mapped with contours, for all reference depths less than or equals to 46 km. I have not considered depths deeper than 46 km, because resolution of these depths is poor, as it can be seen in Figure10b; therefore, the results obtained to these depths can be considered doubtful.

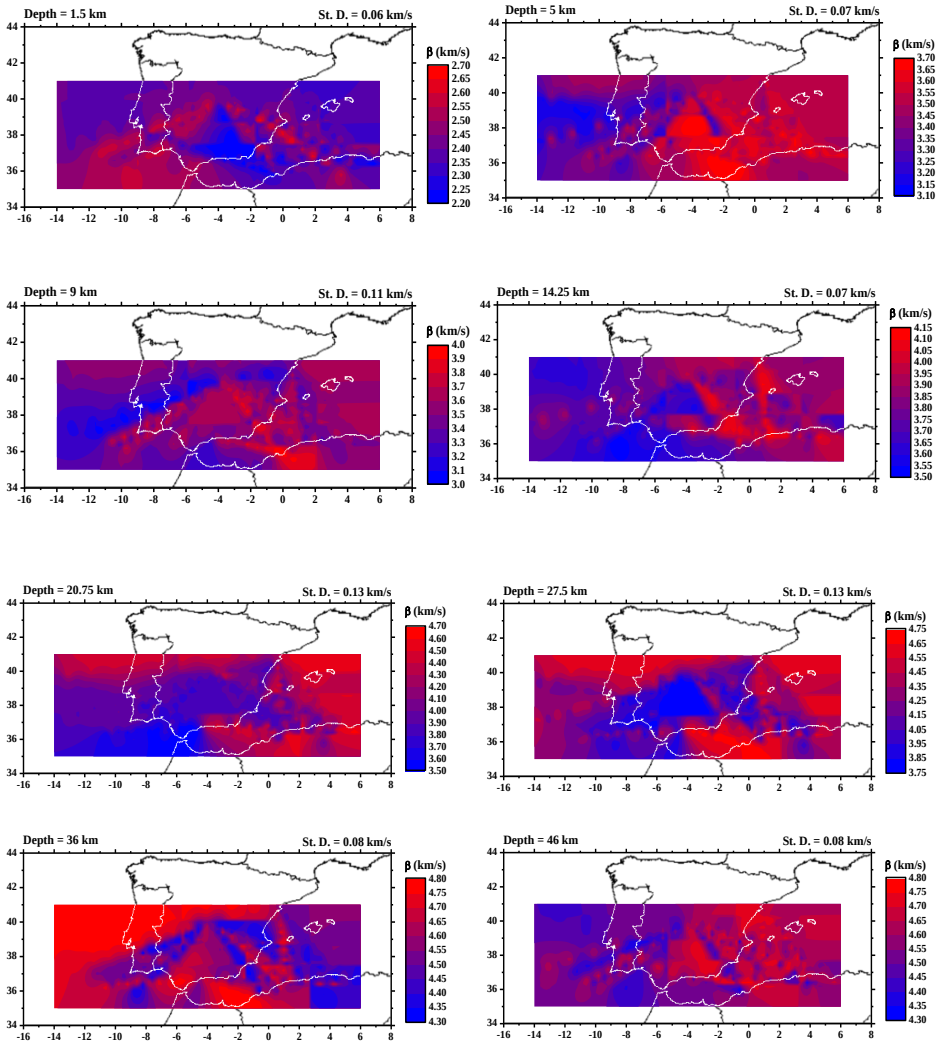

Fig. 12. Shear velocity mapping obtained from the source-station shear velocities after interpolation by kriging. On the left upper corner of the plates, are showed the reference depths. On the right upper corner, are showed the standard deviations obtained for these reference depths.

CONCLUSIONS

Results presented in this paper show the techniques used here as a powerful tool to investigate the structure of crust and upper mantle, through dispersion analysis and shear velocity mapping. By means of these techniques are revealed the principal structural features of the

South Iberia and surroundings zones. Such features are the existence of lateral and vertical heterogeneity in whole study area, as it is concluded when we can see Figure 12; in which, I show a general picture of lithospheric structure from 1.5 to 46 km. In general, the old geological formations of the Iberia show a greater shear velocity than the younger formations. Also it is appreciated that higher velocity values appear in the zones with more shallow Moho depth. This effect can be seen easily, if a Moho depth mapping is carry out to the study zone. To do this, I have taken for each point of regular grid defined in previous section, the depth in which shear velocity is greater than 4.0 km/s, constructing a matrix of Moho depths that can be plotted later. This matrix plotted with contours in Figure 13a. Figures 13b, 13c and 13d; show profiles in several directions that allow appreciating the different ways to make thin of crust. In general, continental crust has a media thickness of 31 km, while marine crust is thinner with a media thickness of 15 km. Some degree of heterogeneity also can be appreciated also in Moho depths distribution.

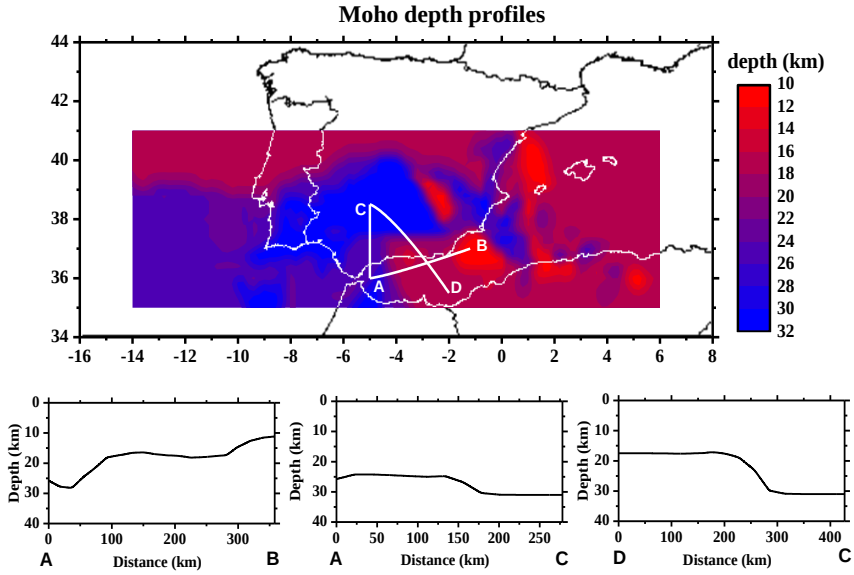

Fig. 13. (a) Moho depth mapping obtained from the shear velocity grids plotted in Figure 12. (b) Vertical cut of the Moho discontinuity from A to B, along the path plotted in Figure 13a. (c) Vertical cut of the Moho discontinuity from A to C. (d) Vertical cut of the Moho discontinuity from D to C.

REFERENCES

Aki K. & P. G. Richards. 1980. *Quantitative Seismology. Theory and methods*. W. H. Freeman and Company, San Francisco.

Badal, J., V.Corchete, G. Payo, J. A. Canas, L. Pujades & F. J. Serón. 1990. *Processing and inversion of long-period surface-wave data collected in the Iberian Peninsula.* Geophys. J. Int.,100, 193-202.

Badal, J., V. Corchete, G. Payo, F. J. Serón, J. A. Canas & L. Pujades. 1992. *Deep structure of the Iberian Peninsula determined by Rayleigh wave velocity dispersion.* Geophys. J. Int.,108, 71-88.

Badal, J., V. Corchete, G. Payo, L. Pujades & J. A. Canas. 1996. *Imaging of Shear-wave velocity structure beneath Iberia.* Geophys. J. Int., 124, 591-611.

Cara, M., 1973. *Filtering dispersed wavetrains.* Geophys. J. R. astr. Soc., 33, 65-80.

Chourak M., Badal J., Corchete V. and Serón F. J., 2001. *A survey of the shallow structure beneath the Alboran Sea using Rg-waves and 3D imaging.* Tectonophysics, 335, 255-273.

Chourak, M., V. Corchete, J. Badal, F. J. Serón & F. Soria. 2003. *Imaging of the Near-Surface Shear-Wave Velocity Structure of the Granada Basin (Southern Spain).* Bulletin of the Seismological Society of America, 93, No. 1, 430-442.

Corchete, V., J. Badal, G. Payo & F. Serón. 1989. *Filtering of dispersed seismic waves.* Rev. De Geofísica, 45, 39-58.

Corchete, V., J. Badal, L. Pujades & J. A. Canas. 1993. *Shear velocity structure beneath the Iberian Massif from broadband Rayleigh wave data.* Phys. Earth Planet. Inter., 79, 349-365.

Corchete, V., J. Badal, F. J. Serón & A. Soria. 1995. *Tomographic images of the Iberian subcrustal lithosphere and asthenosphere*. Journal of Geophysical Research, 100, pp. 24133-24146.

Davis, J. C. 1986. *Statistics and Data Analysis in Geology*. John Wiley & Sons Inc., Second Edition.

Dziewonski, A., S. Bloch, & M. Landisman. 1969. *A technique for the analysis of transient seismic signals.* Bulletin of the Seismological Society of America, 59, No. 1, 427-444.

Navarro, M., V. Corchete, J. Badal, J. A. Canas, L. Pujades & F. Vidal. 1997. *Inversion of Rg Waveforms Recorded in Southern Spain.* Bulletin of the Seismological Society of America, 87, No. 4, pp. 847-865.

Payo, G. 1965. *Iberian Peninsula crustal structure from surface waves dispersion.* Bull. seism. Soc. Am., 55, 727.

Tarantola, A. 1987. *Inverse problem theory. Methods for data fitting and model parameter estimation*. Elsevier, Amsterdam.

ACKNOWLEDGEMENTS

Author is grateful to the geophysical observatories located at Toledo (TOL), Málaga (MAL) and Ebro (EBR); whose have provided the data used for this research. This research was partially supported by the Dirección General de Investigación, Ministerio de Ciencia y Tecnología, Spain, Project BTE2003-00974 (financed with FEDER funds).

Recibido mayo de 2004, aceptado diciembre de 2005.